Power Engineering and Engineering Thermophysics
https://www.acadlore.com/journals/PEET

Experimental and Thermodynamic Assessment of Trickle Solar Preheating in a Small-Scale Geothermal Organic Rankine Cycle

Nugroho Agung Pambudi[1*], Suharno[1], Indra Mamad Gandidi[2]

[1] Department of Mechanical Engineering Education, Universitas Sebelas Maret, 57126 Surakarta, Indonesia
[2] Conversion and Conservation Energy Laboratory, Department of Chemical Engineering, Universitas Pendidikan Indonesia, 40154 Bandung, Indonesia

[*] Correspondence: Nugroho Agung Pambudi (agung.pambudi@staff.uns.ac.id)

Received: 06-13-2026 **Revised:** 08-16-2026 **Accepted:** 09-09-2026

Citation: N. A. Pambudi, Suharno, and I. M. Gandidi, "Experimental and thermodynamic assessment of trickle solar preheating in a small-scale geothermal organic Rankine cycle," *Power Eng. Eng. Thermophys.*, vol. 5, no. 4, pp. 264–281, 2026. https://doi.org/10.56578/peet050402.

© 2026 by the author(s). Published by Acadlore Publishing Services Limited, Hong Kong. This article is available for free download and can be reused and cited, provided that the original published version is credited, under the CC BY 4.0 license.

Abstract: Geothermal brine retains considerable thermal energy before reinjection, but its potential for additional power generation is not always fully utilized. Low-temperature solar preheating offers a possible route to increase heat recovery without altering the geothermal source conditions. This study investigates the integration of a field-tested trickle solar collector as a preheater for a small-scale geothermal organic Rankine cycle (ORC), with particular attention to energy performance, exergy efficiency, heat-transfer feasibility, and working-fluid selection. A thermodynamic model was developed using experimental collector data and a geothermal brine stream entering at 188 °C and leaving at the 90 °C reinjection limit. The brine mass flow rate was fixed at 1.690 kg/s, corresponding to a pinch-feasible 100-kW n-pentane reference cycle. Heat-transfer feasibility was evaluated over the complete counter-current temperature profile using a minimum approach temperature of 10 K. The tested collector produced an average useful heat output of 752.4 W per module and reached a maximum outlet temperature of 51.5 °C. A field of 88 modules, with a total aperture area of 91.52 m^2, supplied 45.024 kW of useful solar heat to the preheater. For the n-pentane cycle, solar preheating increased the net power output from 100 to 106.473 kW while the thermal efficiency remained at 14.377%. The exergy efficiency increased from 51.393% to 53.705%, and the minimum temperature approach remained feasible at 10.120 K. Under the same brine and pinch constraints, R245fa produced the highest net power of 110.961 kW, closely followed by R1233zd(E) at 110.547 kW. Preliminary heat-exchanger sizing yielded a logarithmic mean temperature difference of 12.757 K, a UA value of 3.529 kW/K, and a required heat-transfer area of 7.06–11.76 m^2. The results indicate that trickle collectors are better suited to low-temperature preheating than direct ORC evaporation. This integration provides a technically feasible approach to increasing power recovery from geothermal brine while maintaining the original reinjection temperature and thermodynamic operating limits.

Keywords: Geothermal energy; Organic Rankine cycle; Trickle solar collector; Solar preheating; Heat-transfer matching; Exergy efficiency; Working-fluid selection

1 Introduction

Geothermal energy provides a stable source of renewable electricity because its heat supply is largely independent of short-term weather conditions [1]. In a single-flash geothermal power plant, separated steam drives the main turbine, while the remaining hot brine retains substantial thermal energy and exergy before reinjection. This residual heat can be considered an additional energy resource when it can be recovered without interfering with the main plant. Previous assessments have demonstrated the technical potential of combining geothermal resources with solar heat, although the achievable benefit depends strongly on the site, plant configuration, and operating conditions [1, 2]. Geothermal brine should therefore be regarded not only as a residual fluid requiring reinjection but also as a medium-temperature heat source that may support additional electricity generation.

The organic Rankine cycle (ORC) is well suited to converting low- and medium-temperature geothermal heat into electricity. Recent reviews of geothermal-solar hybrid systems have emphasized the importance of working-fluid selection, heat-source temperature, and thermal integration [2, 3]. Astolfi et al. [4] analyzed a solar-geothermal hybrid plant based on a supercritical ORC and showed that the solar field and operating conditions strongly affected annual productivity and the cost of the additional electricity. Bist and Sircar [5] retrofitted evacuated-tube collectors into a low-enthalpy geothermal ORC and reported power generation of 20–35 kW under the evaluated seasonal conditions. For geothermal water at 80–100 °C, Hu et al. [6] modeled five ORC working fluids and found that R245fa had a slight advantage in net power per unit mass of geothermal water. These studies confirm that geothermal ORC performance remains constrained by source temperature, working-fluid properties, operating conditions, and temperature matching between the brine and the working fluid.

Working-fluid selection and cycle configuration are particularly important when the heat-source temperature approaches the critical range of candidate fluids. Zhang et al. [7] compared subcritical and transcritical cycles for low-temperature geothermal power generation using thermal, exergy, heat-recovery, heat-exchanger, and economic criteria. For geothermal sources at 150–180 °C, Liu et al. [8] found that supercritical-cycle performance was highly sensitive to the selected working fluid and turbine inlet conditions. A meaningful comparison of subcritical and supercritical operation must therefore account for fluid-specific operating conditions and the temperature compatibility between the heat source and the working fluid [2, 7, 8].

Solar heat can be incorporated into a geothermal ORC to increase power production without increasing geothermal brine consumption. Hu et al. [9] investigated the lifetime off-design operation and thermo-economic optimization of a hybrid geothermal-solar power system. Bozkurt et al. [10] also analyzed a low-temperature geothermal-solar integrated system for power and hydrogen generation, while Ge et al. [11] examined the thermodynamic and economic optimization of a combined geothermal-solar power system. Li et al. [12] analyzed a 300-kW solar-geothermal hybrid ORC and reported a maximum increase of 25.34% in annual energy production and a maximum decrease of 16.28% in levelized cost of energy. Podlasek et al. [13] proposed an Artificial Neural Network (ANN)-based model-free control and optimization algorithm for a hybrid ORC plant operating with an unstable heat source. Ghasemi et al. [14] validated a hybrid solar-geothermal ORC model using 7,200 operating data points and reported a maximum second-law-efficiency improvement of approximately 3.4%. Ayub et al. [15] reported a 5.5–6.3% net-power increase at a solar share of approximately 7%, together with a 2% reduction in levelized electricity cost. Shaghaghi et al. [16] analyzed an integrated solar–geothermal ORC from energy, exergy, and thermoeconomic perspectives, including the effects of pinch and evaporation temperatures. Collectively, these findings establish the potential of solar-geothermal integration, particularly when solar heat is introduced at a temperature level compatible with the working-fluid preheating or heating process.

Most solar-assisted geothermal ORC studies have employed medium- or high-temperature solar technologies, including parabolic trough collectors and evacuated-tube collectors. Atiz et al. [17] investigated a 100-m^2 evacuated-tube collector integrated with low-grade geothermal resources at 63–86 °C and reported maximum overall energy and exergy efficiencies of 6.92% and 21.06%, respectively, using n-butane. Erdogan et al. [18] found that the minimum heat-transfer surface area of a heat exchanger increased from 2.644 to 8.681 m^2 as solar irradiance increased from 450 to 1,000 W/m^2. Albrai et al. [19] reported that solar collectors contributed 58% of the total exergy destruction in a solar-geothermal hybrid ORC, whereas Alibaba et al. [20] reported a corresponding contribution of approximately 56% for a geothermal-solar ORC plant. Recent work has also examined Phase Change Material (PCM)-based thermal management in photovoltaic-thermal systems [21] and waste-heat recovery technologies for solid oxide fuel cell/gas turbine (SOFC/GT) hybrid systems [22]. Although concentrated and evacuated-tube collectors can provide the temperatures required for advanced cycle arrangements, their use may increase investment requirements, heat-exchanger duties, system complexity, and collector-related exergy destruction.

Trickle flat-plate collectors provide a different option for supplying low-temperature solar heat. Water flows under gravity across an exposed absorber surface, removing the need for pressurized absorber tubes or synthetic heat-transfer fluids. Pambudi et al. [23] experimentally examined several trickle collector configurations under outdoor conditions in Indonesia and reported that a V-corrugated zinc absorber achieved an overall efficiency of 50% at a flow rate of 120 L/h. Pambudi et al. [24] tested a modified V-corrugated zinc collector in an open solar-water-heating system and reported that flow rate affected its thermal performance. These studies share the basic heat-transfer mechanism of direct contact between a thin water film and the absorber surface, but the present work extends the application to solar preheating for a geothermal ORC.

The available experimental evidence indicates that trickle collectors can produce useful low-temperature heat through a relatively simple, non-pressurized configuration. However, their role in geothermal power systems has not been established. Previous solar-geothermal ORC studies have generally relied on medium- or high-temperature collectors, simulated collector performance, or manufacturer data. Experimental output from a trickle collector has not been directly incorporated into a geothermal ORC model to determine how much of the collected heat can be transferred under realistic temperature constraints. It also remains unclear whether the low collector outlet temperature permits a meaningful increase in ORC power, how solar preheating changes the energy and exergy performance of the system, and whether the result remains thermodynamically feasible when the complete counter-current temperature profile is examined rather than only the terminal temperatures. Recent reviews of combined-source ORCs and studies of flat-plate solar ORCs emphasize heat-source compatibility and operating-condition optimization [25, 26]. Nevertheless, an experimentally grounded assessment of low-temperature trickle preheating for a geothermal ORC is still lacking.

This study investigates the integration of a field-tested trickle solar collector as a preheater for a small-scale geothermal ORC. The collector measurements are used directly as the solar-side input to the thermodynamic model, avoiding reliance on simulated collector performance or manufacturer specifications. A geothermal-only ORC and a solar-preheated ORC are compared at the same brine inlet temperature and mass flow rate to determine the changes in net power, thermal efficiency, and exergy efficiency. The analysis also examines hypothetical collector outlet temperatures of 55–65 °C to distinguish the effect of a wider preheating temperature range from that of additional useful solar heat. Heat-transfer feasibility is verified along the complete counter-current heating profile by imposing a common minimum temperature approach. Several working fluids are then compared under the same geothermal brine and pinch constraints in subcritical and supercritical operation, while transcritical CO_2 is included as a limiting case for an intermediate-temperature geothermal source. In addition, preliminary preheater sizing is performed to connect the thermodynamic results with heat-exchanger requirements. The study thus provides an experimentally based assessment of low-temperature solar preheating and clarifies the conditions under which a trickle collector can increase power recovery from geothermal brine without changing the prescribed reinjection temperature.

2 Methodology

2.1 System Description and Analysis Boundaries

Figure 1 shows the plant layout and the calculation boundary adopted in this study. The system studied in the analysis was a small-scale binary ORC supplied with separated brine from a geothermal power plant, combined with trickle solar collectors as a preheater. The system consisted of three main loops, namely a geothermal fluid, a trickle solar collector, and a working fluid. On the geothermal side, fluid from the production well entered the separator. The separated steam was used to drive the main steam turbine, while the hot liquid brine served as a heat source for the ORC evaporator before being channeled to the reinjection well. The production well, separator, main steam turbine, and geothermal generator fall outside the calculation boundary and are excluded from all energy, power, thermal-efficiency, and exergy-efficiency results. The calculation boundary starts at the brine stream delivered to the binary heat exchanger and contains the collector-water loop, the solar preheater, the ORC pump, the geothermal evaporator, the expander, and the condenser. On the ORC side, the working fluid was pumped from condensation pressure to evaporation pressure, preheated in the preheater by heat from the trickle collector, then further heated in the evaporator by geothermal brine. Following the process, the fluid was expanded in the ORC expander/turbine to generate power, and later condensed in the condenser.

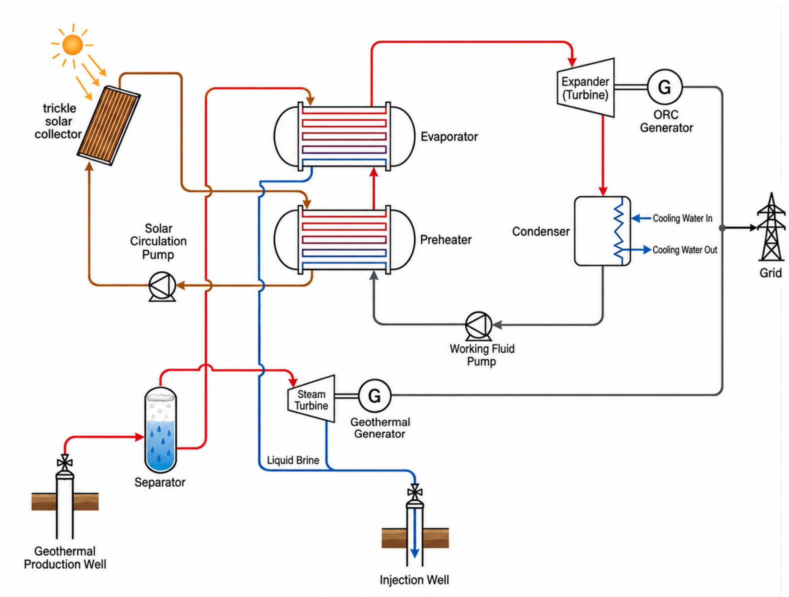

Figure 1. Schematic diagram of the hybrid geothermal–organic Rankine cycle (ORC) system with a trickle solar collector as a preheater

The geothermal brine data used as the basis for the simulation were the characteristics of a medium-temperature geothermal field brine with an inlet temperature of 188 °C, cooled to a reinjection limit temperature of 90 °C. The brine mass flow rate was calibrated to 1.690 kg/s, at which the optimized n-pentane reference case that satisfied the full-profile minimum approach produced a net output of 100 kW. That single flow rate was then held fixed for every other scenario and working fluid, and no fluid was rescaled to reproduce 100 kW. The 100 kW value is therefore a calibrated reference point for one fluid, not an output imposed on the whole comparison. This method was used to assess additional power to be obtained from the same geothermal brine. The use of residual brine from single-flash geothermal systems was also relevant because the brine transported thermal energy before reinjection. The available heat from the brine was calculated during the process as follows.

$$\dot{Q}_{\text{brine}} = \dot{m}_{\text{brine}} \left(h_{\text{brine,in}} - h_{\text{brine,out}}\right) \tag{1}$$

where, $\dot{m}_{\text{brine}}$ is the brine mass flow rate (kg s^{-1}), $h_{\text{brine,in}}$ and $h_{\text{brine,out}}$ are the inlet and outlet specific enthalpies (kJ kg^{-1}), and $\dot{Q}_{\text{brine}}$ is the heat released by the brine (kW). The model assumes steady-state operation and neglects pressure drops in the piping and heat exchangers and heat loss to the environment. For a consistent comparison across working fluids, the turbine isentropic efficiency, pump efficiency, and organic-fluid condensation temperature were set to 0.80, 0.75, and 30 °C, respectively. These are adopted model settings.

2.2 Trickle Solar Collector Experimental Data

Trickle solar collector performance data were obtained from field experiments conducted under actual outdoor conditions. A V-shaped wave solar collector with a trickle flow system was used, where water was circulated from the reservoir tank to the absorber surface, flowed by gravity over the absorber, and then returned to the reservoir. Moreover, the collector used a single transparent glass cover and a V-corrugated zinc absorber. The assembled collector and the instruments used during the tests are shown in Figure 2. The physical specifications of the collector used in the tests are shown in Table 1.

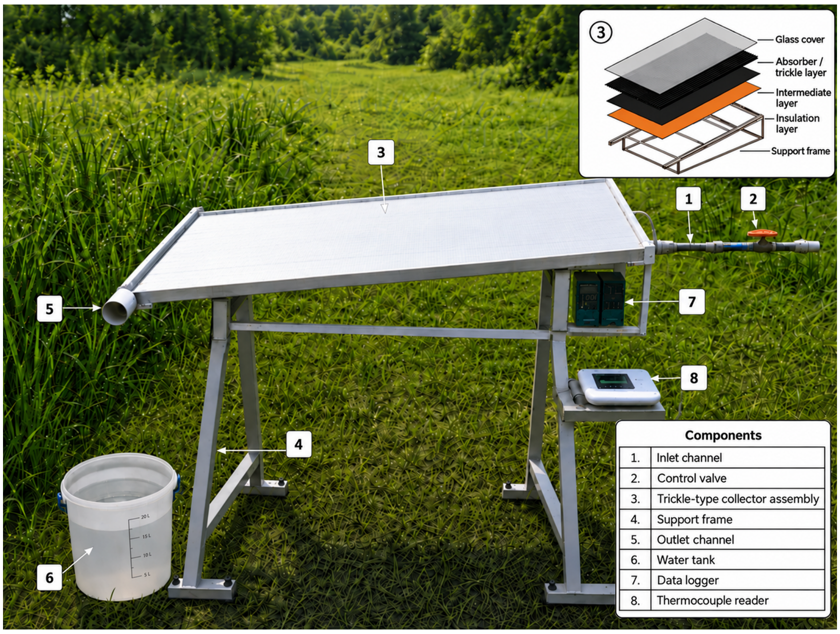

Figure 2. Experimental setup of the trickle solar collector and the main components of the testing system

Tests were conducted at three flow rate variations, including 2, 3, and 4 L/min. Inlet temperature, outlet temperature, and solar irradiance were recorded during the test period from 9:00 AM to 12:00 PM using a data logger as well as a thermocouple reader. A flow rate of 4 L/min was selected as the primary input for the ORC model because it produced the highest average useful heat compared to other flow rate variations. The experimental data for the trickle collector were previously reported in V-corrugated collector testing, where the trickle collector structure showed potential as a simple, gravity-driven solar water heater [23]. The useful heat generated by the collector was calculated using the following equation.

$$\dot{Q}_u = \dot{m}_w c_{p,w} \left(T_{\text{out}} - T_{\text{in}}\right) \tag{2}$$

where, $\dot{Q}_u$ is useful collector heat (W), $\dot{m}_w$ is water mass flow rate (kg s^{-1}), $c_{p,w}$ is the specific heat capacity of water (J kg^{-1} K^{-1}), and T_{out} and T_{in} are the collector outlet and inlet temperatures. The useful heat density was calculated during the process using the following equation.

$$q_u'' = \frac{\dot{Q}_u}{A_c} \tag{3}$$

Table 1. Physical specifications of the trickle solar collector

Parameter	Value
Collector length	1.3 m
Collector width	0.8 m
Collector aperture area	1.04 m^2
Absorber/collector thickness	0.2 mm
Absorber thermal conductivity	116 W/mK
Absorber absorptivity	0.969
Absorber emissivity	0.969
Absorber-to-glass-cover gap	2 cm
Transparent glass-cover thickness	0.3 cm
Glass-cover transmissivity	0.79
Glass-cover emissivity	0.90
Collector insulation thickness	0.3 cm
Insulation thermal conductivity	0.00016 W/mK

The collector thermal efficiency was also calculated using the following equation.

$$\eta_{\text{col}} = \frac{\dot{Q}_u}{A_c G_T} \tag{4}$$

where, q''_u is collector useful heat flux, A_c is the collector aperture area (m^2), G_T is incident solar irradiance (W m^{-2}), and η_{col} is collector thermal efficiency (dimensionless). In the ORC model, the experimental parameters used directly were the average useful heat per module, the maximum collector outlet temperature, and the collector aperture area. The optical and thermal parameters in Table 1 were used to describe the characteristics of the test equipment and strengthen the replicability of the experiment.

2.3 Collector Heat Calculation and Solar Field Scaling

The useful heat per module was scaled to the collector field to integrate trickle collectors into an ORC system. The number of collector modules required to supply the target heat of the preheater was calculated as follows.

$$N_{\text{modul}} = \frac{\dot{Q}_{\text{target}}}{\dot{Q}_{\text{modul}}\, f_{\text{derating}}\, \varepsilon_{\text{HX}}} \tag{5}$$

where, N_{modul} is the number of collector modules, $\dot{Q}_{\text{target}}$ represents the target solar heat supplied to the preheater, and $\dot{Q}_{\text{modul}}$ is the average useful heat per module. f_{derating} represents the derating factor to account for pipe losses and irradiance variations, and ε_{HX} is the effectiveness of the heat exchanger between the collector loop and the ORC working fluid. In this study, f_{derating} was set at 0.85 and ε_{HX} at 0.80. Both values are engineering screening assumptions rather than measured constants, because the field piping, storage arrangement, and preheater geometry of a full installation were not built in this work. To avoid presenting them as fixed truths, a two-factor sensitivity was carried out over f_{derating} = 0.75, 0.85, and 0.95 and ε_{HX} = 0.70, 0.80, and 0.90, and the resulting spread in net power is reported in the Results section.

The preheating temperature limit was determined by the collector outlet temperature and the minimum temperature difference in the heat exchanger. The maximum working fluid temperature after the preheater was calculated as follows.

$$T_{\text{WF,max}} = T_{\text{solar,out}} - \Delta T_{\min} \tag{6}$$

where, $T_{\text{solar,out}}$ is the collector outlet temperature, and $\Delta T_{\min}$ is the specified minimum temperature difference in the heat exchanger. The value of $\Delta T_{\min}$ was set at 5 °C. The heat transferred to the cycle is the smaller of the collector-side available heat and the heat accepted before this temperature limit is reached.

$$SF = \frac{\dot{Q}_{\text{solar}}}{\dot{Q}_{\text{total}}} \times 100\% \tag{7}$$

$$SF_{\text{brine}} = \frac{\dot{Q}_{\text{solar}}}{\dot{Q}_{\text{brine}}} \times 100\% \tag{8}$$

where, SF and SF_{brine} are solar fractions, $\dot{Q}_{\text{solar}}$ is the solar heat supplied to the preheater, $\dot{Q}_{\text{total}}$ is the heat supplied by the geothermal brine.

2.4 Organic Rankine Cycle Thermodynamic Modeling Based on Python Programming

The ORC thermodynamic model used in this study was developed in Python. The thermodynamic properties of the working fluid were calculated using CoolProp [27]. Moreover, data processing, numerical calculations, and visualization were performed using appropriate Python libraries. This model was used to calculate cycle state points, working fluid mass flow rate, turbine work, pump work, net power, thermal efficiency, and system exergy parameters.

The ORC cycle used during the analysis consisted of five main state points. State 1 was the condenser outlet as saturated liquid at the condensation temperature. State 2 was the pump outlet at evaporation pressure, and State 3 was the preheater outlet after receiving heat from the trickle collector. Additionally, State 4 represented the turbine inlet/expander after receiving the main heat input from the geothermal brine in the evaporator. State 5 was the turbine outlet/expander before entering the condenser. This basic configuration was commonly used in geothermal ORC evaluations because the formation allowed analysis of the effects of heat source temperature, evaporation pressure, and working fluid on the net power of the system [7, 8]. The pump conditions were calculated using the isentropic method as follows.

$$h_{2s} = h_1 + \frac{P_2 - P_1}{\rho_1} \tag{9}$$

$$h_2 = h_1 + \frac{h_{2s} - h_1}{\eta_{\text{pump}}} \tag{10}$$

where, h_{2s} is the isentropic pump outlet enthalpy, and h_2 represents the actual pump outlet enthalpy. P_1 and P_2 are the low- and high-side pressures, ρ_1 represents the working fluid density at the condenser outlet, and η_{pump} is the isentropic efficiency of the pump. The expansion process in the turbine/expander was calculated as follows.

$$s_{5s} = s_4 \tag{11}$$

$$h_5 = h_4 - \eta_{\text{turb}} \left(h_4 - h_{5s}\right) \tag{12}$$

where, h_{5s} is the turbine outlet enthalpy in the isentropic process, and h_5 represents the actual turbine outlet enthalpy. s_4 is the entropy of the working fluid at the turbine inlet, and η_{turb} represents the turbine isentropic efficiency.

The mass flow rate of the working fluid was calculated based on the total heat input to the cycle:

$$\dot{Q}_{\text{total}} = \dot{Q}_{\text{brine}} + \dot{Q}_{\text{solar}} \tag{13}$$

$$\dot{m}_{\text{WF}} = \frac{\dot{Q}_{\text{total}}}{h_4 - h_2} \tag{14}$$

For the brine-only ORC scenario, $\dot{Q}_{\text{total}}$ was derived from geothermal brine. For the ORC scenario with a trickle preheater, $\dot{Q}_{\text{total}}$ was the sum of the geothermal brine heat and the solar heat supplied through the preheater. During the process, turbine work, pump work, and net power were calculated as follows.

$$\dot{W}_{\text{turb}} = \dot{m}_{\text{WF}} \left(h_4 - h_5\right) \tag{15}$$

$$\dot{W}_{\text{pump}} = \dot{m}_{\text{WF}} \left(h_2 - h_1\right) \tag{16}$$

$$\dot{W}_{\text{net}} = \dot{W}_{\text{turb}} - \dot{W}_{\text{pump}} \tag{17}$$

$$\Delta\dot{W}_{\text{net}} = \dot{W}_{\text{net,trickle}} - \dot{W}_{\text{net,ORC}} \tag{18}$$

$$PG = \frac{\Delta\dot{W}_{\text{net}}}{\dot{W}_{\text{net,ORC}}} \times 100\% \tag{19}$$

where, $\dot{W}$ denotes the power/work rate, PG is the net power gain, and $\Delta\dot{W}_{\text{net}}$ is the net power difference.

The thermal efficiency of the cycle was calculated by the following equation.

$$\eta_{\text{th}} = \frac{\dot{W}_{\text{net}}}{\dot{Q}_{\text{total}}} \tag{20}$$

$$w_{\text{net,brine}} = \frac{\dot{W}_{\text{net}}}{\dot{m}_{\text{brine}}} \tag{21}$$

where, $w_{\text{net, brine}}$ is specific net power per brine mass flow rate.

The Python model was operated iteratively for each system scenario, evaporation temperature, working fluid, and preheater condition. This method compared all scenarios on the same geothermal brine basis, allowing differences in power output to be attributed to the presence of the preheater, collector temperature, and working fluid selection. A hot-end temperature check alone is not sufficient, because the smallest temperature difference between the brine and the working fluid can occur inside the heating profile rather than at either endpoint. For that reason, the brine and working-fluid temperatures were evaluated at 401 equal heat-duty fractions x over the complete counter-current profile, and a case was accepted only when the minimum approach along that whole profile satisfied $\Delta T_{\text{min,calc}}$ 10 K for both the brine-only and the solar-assisted conditions. Here, x is the normalized heat-duty fraction evaluated at 401 equally spaced points across the complete counter-current heating profile.

2.5 Exergy Analysis

Exergy analysis was conducted to evaluate the energy usage quality of geothermal brine and solar heat. This analysis was important because adding low-temperature heat does not necessarily produce the same improvement in energy-conversion quality as adding higher-temperature heat. The exergy method has been widely used in combined-source ORC assessments to quantify second-law efficiency and component exergy destruction [25]. During the process, the ambient/dead-state temperature was set to 298.15 K. The physical exergy released by the brine during the cooling process from the inlet to the reinjection temperature was calculated as follows.

$$\dot{E}x_{\text{brine}} = \dot{m}_{\text{brine}} \left[(h_{\text{in}} - h_{\text{out}}) - T_0 (s_{\text{in}} - s_{\text{out}})\right] \tag{22}$$

where, $\dot{E}x$ is exergy rate, h_{in} and s_{in} represent the enthalpy and entropy of the brine at the inlet conditions, h_{out} and s_{out} are the enthalpy and entropy of the brine at the reinjection temperature.

The exergy of solar heat entering through the preheater was calculated based on the Carnot factor of the heat source as follows.

$$\dot{E}x_{\text{solar}} = \dot{Q}_{\text{solar}} \left(1 - \frac{T_0}{T_{\text{solar}}}\right) \tag{23}$$

$$\dot{E}x_{\text{in,total}} = \dot{E}x_{\text{brine}} + \dot{E}x_{\text{solar}} \tag{24}$$

where, $\dot{Q}_{\text{solar}}$ is the solar heat supplied to the preheater, and T_{solar} is the absolute temperature of the solar heat source used in the heat exchanger, T_0 is the dead-state temperature, and $\dot{E}x_{\text{in,total}}$ is total exergy input. The exergy efficiency of the system during the process was calculated as follows.

$$\eta_{\text{ex}} = \frac{\dot{W}_{\text{net}}}{\dot{E}x_{\text{brine}} + \dot{E}x_{\text{solar}}} \tag{25}$$

For the brine-only ORC scenario, $\dot{E}x_{\text{solar}} = 0$, allowing the exergy input to be obtained only from geothermal brine. For the ORC scenario with a trickle preheater, the exergy input was the sum of the brine exergy and solar exergy. The total exergy destruction of the system was calculated from the difference between the total exergy input and the net power generated.

$$\dot{E}x_{\text{dest}} = \dot{E}x_{\text{in}} - \dot{W}_{\text{net}} \tag{26}$$

$$\psi_{\text{dest}} = \frac{\dot{E}x_{\text{dest,total}}}{\dot{E}x_{\text{in,total}}} \times 100\% \tag{27}$$

This analysis was used to differentiate the increase in power due to additional heat input from the increase in the quality of energy usage.

2.6 System Simulation Scenario

This study used several simulation scenarios to evaluate the effects of a trickle preheater, increased collector temperature, working fluid selection, and cycle operation mode on the performance of a geothermal ORC. The first scenario was a brine-only ORC that used geothermal brine as its sole heat source. The second scenario was an ORC with a trickle preheater, based on actual experimental data from a collector with a collector outlet temperature of 51.5 ℃. In the scenario, solar heat was provided during the initial heating stage of the working fluid before it entered the geothermal evaporator.

Two additional parametric scenarios were used to evaluate potential collector performance improvements. The improved collector scenario used a collector outlet temperature of 55 ℃, while the advanced collector scenario applied a collector outlet temperature of 65 ℃; both were technology-development scenarios. In practice, higher outlet temperatures might be pursued through measures such as adding reflectors, using selectively coated absorbers, optimizing airflow rates, improving thermal insulation, or applying a partially transparent cover to reduce convective losses. These measures are illustrative development options only; none was evaluated experimentally in the present study. A review of the simulation scenarios used in this study is shown in Table 2.

Table 2. Scenarios for the geothermal-trickle organic Rankine cycle (ORC) system

Scenario	Description	Objective
S1	ORC without solar preheater	Establish baseline performance from geothermal brine
S2	ORC with trickle preheater based on 51.5 ℃ experimental data	Evaluate the actual trickle collector contribution
S3	ORC with improved trickle collector at 55 ℃	Assess moderate collector performance improvement
S4	ORC with advanced trickle collector at 65 ℃	Assess further trickle collector development potential
S5	Multi-fluid comparison under subcritical operation	Rank six organic working fluids on a common basis
S6	Transcritical CO_2 cycle	Assess the feasibility limit of CO_2 for a 188 ℃ heat source

2.7 Multi-Fluid Analysis and the Transcritical CO_2 Case

A multi-fluid analysis was conducted to evaluate how the trickle preheater contribution remained relevant across different ORC working fluid types. The six working fluids compared were n-butane, R245fa, R1233zd(E), isopentane, cyclopentane, and n-pentane. These fluids were selected based on the representation of several groups of organic fluids commonly used or considered for low- to medium-temperature ORC. n-pentane, isopentane, and cyclopentane represented hydrocarbons for medium-temperature heat sources. R245fa was used as a reference fluid widely applied in ORC studies. In addition, R1233zd(E) was selected as a contemporary ORC candidate, and n-butane represented a fluid with a lower critical temperature.

Each fluid was analyzed in subcritical mode, with an optimum evaporation temperature obtained through a parametric search to maximize thermal efficiency. A separate R1233zd(E) diagram was generated to illustrate subcritical and supercritical thermodynamic paths. For this illustration, supercritical feasibility required the fluid critical temperature to be below the maximum permissible turbine-inlet temperature, as defined below.

$$T_{\text{turb,in,max}} = T_{\text{brine,in}} - \Delta T_{\text{pinch}} \tag{28}$$

where, $T_{\text{turb,in,max}}$ is the maximum working-fluid temperature permitted at the turbine inlet after applying the geothermal inlet temperature and the specified approach constraint.

With a brine inlet temperature of 188 ℃ and a 10 K minimum approach, the maximum permissible turbine-inlet temperature was 178 ℃. The six-fluid common-basis comparison was performed in subcritical mode. For the separate R1233zd(E) illustration, the subcritical and supercritical turbine-inlet temperatures were set to 155 ℃ and 178 ℃, respectively. The supercritical high-side pressure was scanned from 1.03 to 2.0 times the critical pressure, and the point with the greatest specific net work was selected. These illustrative paths were not used in the six-fluid subcritical ranking. Terminal and complete-profile minimum approaches are distinguished throughout the analysis.

As a comparison case, CO_2 was analyzed in a transcritical cycle. CO_2 has a critical temperature of 30.98 ℃, so subcritical condensation requires a condensation temperature below the critical temperature. The condensation temperature of CO_2 was therefore set at 25 ℃, different from the 30 ℃ condensation temperature used for the organic fluids. Because that difference makes the comparison unequal, a second CO_2 case was added at the same 30 ℃ sink used for the organic fluids, and both cases are reported so that the effect of sink temperature can be separated from the effect of the fluid. The high-side pressure of CO_2 was scanned from 1.05 to 3.5 times the critical pressure. In this study, CO_2 was treated as a limiting comparison because its high operating pressure and compression work materially reduced net output under the evaluated geothermal conditions.

3 Results and Discussion

3.1 Trickle Collector Experimental Performance

The performance of the trickle solar collector was evaluated based on field test data at three flow rate variations: 2, 3, and 4 L/min. The collector outlet temperature and solar irradiance profiles during the test period are shown in Figure 3. In general, the collector outlet temperature followed changes in solar irradiance. As irradiance increased toward midday, the collector outlet temperature also improved. The maximum outlet temperature reached 51.5 ℃ at the end of the test period, when solar irradiance was at its highest during the observation time. For integration with the ORC, 51.5 ℃ was treated as the collector hot-water temperature available at the trickle-system outlet and was sent to the preheater.

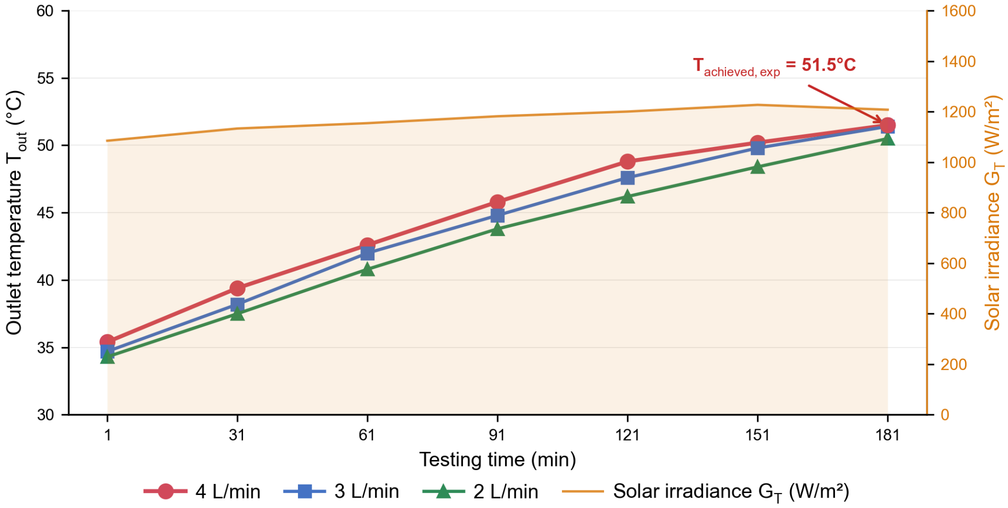

Figure 3. Outlet temperature profile of the trickle collector and solar irradiance during the experiment

At a flow rate of 4 L/min, the collector produced an average useful heat output of 752.4 W per module with an average useful heat flux of 723.5 W/m^2. This value indicated that the trickle collector was capable of providing stable low-temperature heat under field conditions. However, the maximum outlet temperature of 51.5 ℃ also signified that this collector was not suitable for use as the primary heat source for ORC working fluid evaporation. The role was more appropriate as a preheater at the beginning of the working fluid heating process, before the fluid received the main heat input from geothermal brine in the evaporator.

This characteristic is important for understanding the role of trickle technology in a hybrid ORC system. Trickle collectors are not intended to replace geothermal brine but to provide initial heating on the preheating side. Their simple construction, gravity-driven flow, and absence of high-pressure absorber pipes distinguish them from medium- to high-temperature collectors such as parabolic trough and evacuated-tube collectors. No economic comparison among collector types was performed in this study.

3.2 Thermodynamic Limits of Preheating by Trickle Collectors

The ability of the trickle collector as a preheater was limited by the collector outlet temperature. In this study, the maximum collector outlet temperature used was 51.5 ℃. Assuming a minimum temperature difference of 5 ℃ in the heat exchanger, the maximum working fluid temperature after the preheater was approximately 46.5 ℃. This indicated that heat from the trickle collector was only supplied during the initial heating process of the working fluid. After the temperature limit was exceeded, the working fluid was heated by the geothermal brine in the evaporator.

The preheating range that was supplied by the trickle collector was shown in Figure 4. Against the brine duty of 695.556 kW available between 188 ℃ and the 90 ℃ reinjection limit, the solar heat accepted by the working fluid represented 6.080% of the total heat input after preheater integration. Therefore, the trickle collector functioned as a low-temperature preheater, not a solar evaporator.

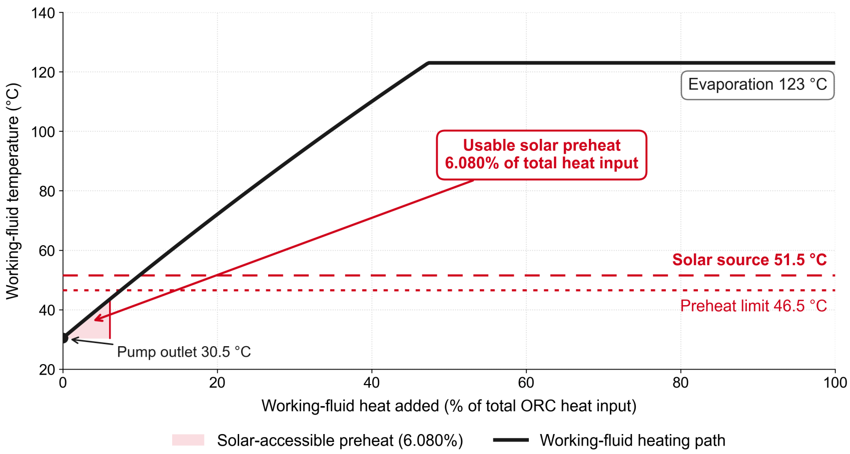

Figure 4. Organic Rankine cycle (ORC) working-fluid preheating range supplied by the trickle collector

The solar contribution limit was the basis for determining the collector field size. After considering derating factors and heat exchanger effectiveness when using the effective heat per module, 88 collector modules, or 91.52 m^2 of collector area, made 45.024 kW of solar heat available on the ORC side. The largest heat the working fluid could accept under the 51.5 °C collector outlet and the 5 °C approach was 56.313 kW for the reference case. Because the available heat was the smaller of the two quantities, the whole 45.024 kW was transferred to the preheater and no collector heat was rejected by the temperature constraint.

3.3 Effect of Trickle Preheater on Organic Rankine Cycle Energy Performance

The brine-only ORC and the ORC with a trickle preheater were compared using n-pentane as the reference working fluid. Both scenarios were analyzed at the same brine mass flow rate of 1.690 kg/s and the same 123 °C evaporation temperature, allowing performance differences to be directly attributed to the solar heat contribution from the trickle collector. The main comparison results are shown in Table 3.

Table 3. Performance comparison between the organic Rankine cycle (ORC) and the ORC with a trickle preheater

Parameter	Brine-Only ORC	ORC With Trickle Preheater
Brine mass flow rate (kg/s)	1.690	1.690
Brine heat input (kW)	695.556	695.556
Solar heat available (kW)	0	45.024
Solar heat transferred (kW)	0	45.024
Total heat input (kW)	695.556	740.579
Working-fluid flow (kg/s)	1.371	1.460
Turbine power (kW)	102.616	109.258
Pump power (kW)	2.614	2.783
ORC net power (kW)	100	106.473
Net power increase (%)	—	6.473
Thermal efficiency (%)	14.377	14.377
Exergy efficiency (%)	51.393	53.705
Minimum approach along profile (K)	13.435	10.120
Brine outlet temperature (°C)	90.0	90.0
Number of trickle modules	0	88

Note: An em dash (—) indicates that the quantity is not applicable to the brine-only reference case.

The addition of a trickle preheater increased the net ORC power from 100 kW to 106.473 kW. Essentially, the system obtained an additional 6.473 kW, or approximately 6.473%, of power from the same geothermal brine. This increase occurred because the 45.024 kW of solar heat improved the total heat input to the cycle, raising the mass flow rate of the circulating working fluid from 1.371 kg/s to 1.460 kg/s.

The thermal efficiency of both scenarios remained the same at 14.377%. This was thermodynamically reasonable because the cycle configuration, evaporation temperature, condensation temperature, and component efficiency remained unchanged. The trickle preheater did not change the upper or lower temperature limits of the cycle, but it increased the amount of heat that the cycle could process. Therefore, the net power increase occurred proportionally to the additional heat input, without changing the thermal efficiency of the cycle. The primary benefit of the trickle preheater in this scenario was increasing the power output capacity from the same brine, without increasing the baseline ORC thermal efficiency.

3.4 Exergy and Temperature-Profile Analysis of the Organic Rankine Cycle–Tickle System

Adding solar heat upstream of the evaporator changes the downstream heat-transfer duty, so the complete counter-current profile was compared for the brine-only and the solar-assisted case in Figure 5. In both cases, the smallest temperature difference occurred inside the geothermal heater/evaporator rather than at either endpoint, which is why a hot-end check alone is not sufficient. The minimum approach decreased from 13.435 K in the brine-only case to 10.120 K with solar assistance because the larger working-fluid flow moves the profile closer to the brine curve; both cases remained feasible against the specified 10 K limit. The brine outlet stayed at the 90 °C reinjection floor in both cases, so the modeled retrofit did not cool the brine further or change the reinjection condition. Mineral-scaling risk was outside the scope of this thermodynamic assessment and was not inferred from temperature alone.

Exergy efficiency increased from 51.393% in the brine-only ORC to 53.705% in the system with a trickle preheater. This improvement indicated more effective use of the combined geothermal and solar exergy inputs. Although the incoming solar exergy was relatively small at 3.675 kW compared with the brine exergy of 194.581 kW, it was supplied during the initial stage of working-fluid heating without increasing the maximum cycle temperature.

These results show that the trickle collector should not be evaluated solely from its relatively low outlet temperature. The collector supplied 45.024 kW of additional heat, increasing the net power recovered from the same geothermal brine by 6.473 kW.

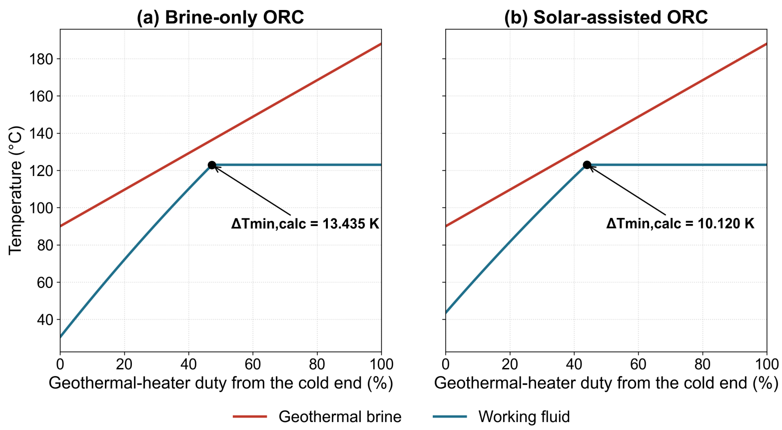

Figure 5. Counter-current temperature profiles for the n-pentane reference case

Note: ORC: organic Rankine cycle.

3.5 Trickle Collector Improvement to 55–65 °C

After evaluating actual experimental conditions at a maximum temperature of 51.5 °C, parametric simulations were conducted to assess the potential for performance improvements when the trickle collector design could be improved. Two additional scenarios were analyzed, namely an improved collector with an outlet temperature of 55 °C and an advanced collector with an outlet temperature of 65 °C. These two scenarios were not treated as actual experimental data, but as projections for technology development.

Increasing the collector temperature expanded the temperature window available to solar heat, but it did not by itself increase the heat the field could deliver. At 51.5 °C the transferable heat was already limited by the 45.024 kW made available by 88 modules, not by the 56.313 kW temperature limit. Raising the assumed collector outlet to 55 °C or 65 °C therefore widened the margin against the temperature constraint while the transferred heat and the net power stayed at the field-limited value. The sensitivity of the result to the collector and exchanger assumptions is shown in Figure 6.

The two-factor sensitivity over collector derating factors of 0.75–0.95 and preheater effectiveness values of 0.70–0.90 gave a net power between 104.998 kW and 108.096 kW, with the central 0.85 and 0.80 case at 106.473 kW. Only the most optimistic combination of 0.95 and 0.90 reached the 56.313 kW temperature limit. The preheater itself was also screened for engineering feasibility at the reference duty of 45.024 kW. The collector water cooled from 51.5 °C to 49.7 °C while n-pentane was warmed from 30.5 °C to 43.5 °C, giving terminal approaches of 7.972 K and 19.156 K, a logarithmic mean temperature difference of 12.757 K, and a required UA of 3.529 kW/K. With a screening overall coefficient of 400 $W/m^2/K$ taken from a preliminary ORC sizing model [28], the required area was 8.82 m^2, rising to 11.76 m^2 at 300 $W/m^2/K$ and falling to 7.06 m^2 at 500 $W/m^2/K$. A vendor-rated design is still required, and it must address plate pattern, flow maldistribution, fouling, pressure drop, material compatibility, and control.

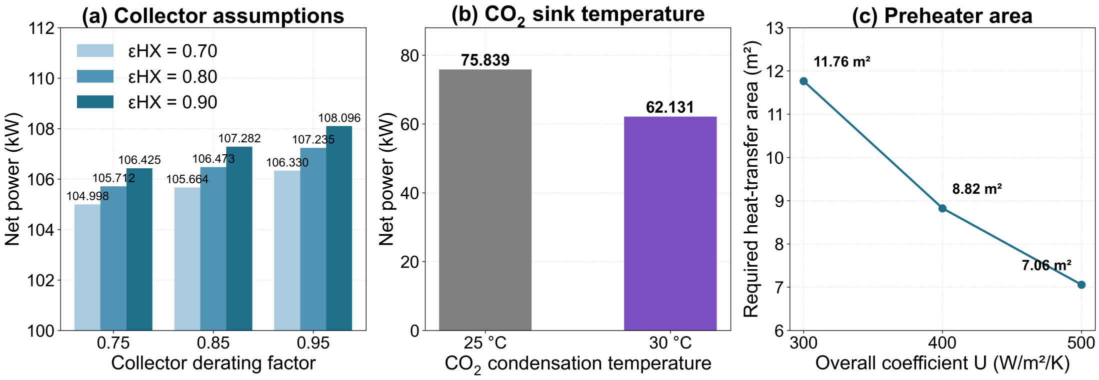

Figure 6. Sensitivity of the solar-assisted result to the main modelling assumptions

The results indicated that a larger power gain requires more useful collector heat, more aperture area, or a higher collector efficiency, because raising the outlet temperature alone does not add energy to the field. Potential measures include adding reflectors, using selective absorber layers, optimizing airflow rates, improving thermal insulation, and applying partially transparent covers. However, any design improvements should maintain the primary advantages of the trickle collector, namely, simple construction, gravity-driven flow, and straightforward operation.

3.6 Effect of Working Fluid Selection on Subcritical Mode

A multi-fluid analysis was conducted to determine how the benefits of the trickle preheater remained relevant across different working fluids. Six fluids, including n-butane, R245fa, R1233zd(E), isopentane, cyclopentane, and n-pentane, were analyzed. All fluids were compared under the same geothermal-brine conditions, as the differences in power output were primarily influenced by the thermodynamic properties of the working fluid, optimum evaporation temperature, and operating pressure.

The results of the working fluid comparison were shown in Figure 7. Every candidate was evaluated at the same brine inlet and outlet temperature, the same brine flow, the same condensation temperature, the same component efficiencies, and the same full-profile 10 K minimum approach. On that common basis, R245fa produced the highest solar-assisted net power at 110.961 kW, followed closely by R1233zd(E) at 110.547 kW, n-butane at 109.987 kW, isopentane at 106.955 kW, n-pentane at 106.473 kW, and cyclopentane at 101.788 kW. Fluids with higher thermal efficiency generated greater additional power from the same solar heat, as the additional power from the preheater was directly proportional to the thermal efficiency of the cycle. Therefore, working fluid selection affected two aspects simultaneously, including the base power from the geothermal brine and the additional power from the trickle preheater.

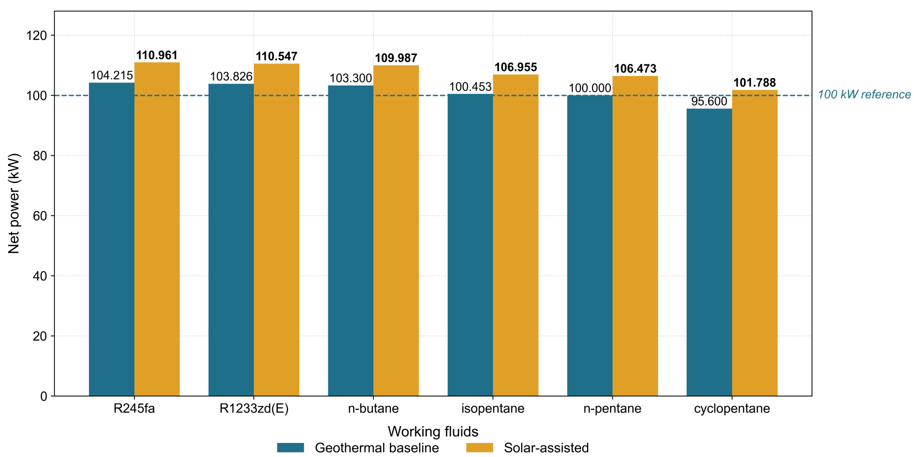

Figure 7. Net power of the six working fluids on the common brine and pinch basis

This common-basis ranking differs from rankings obtained when each fluid is evaluated at an independent operating point and only a hot-end temperature check is applied. On the common basis, cyclopentane reaches its optimum at a lower evaporation temperature of 106 °C and therefore extracts less power from the same brine, while an n-pentane point at 150 °C is infeasible once the complete profile is examined, with calculated minimum approaches of -2.180 K without solar heat and -4.816 K with solar heat. Working-fluid selection should not be based on power output alone. Operating pressure, safety, fluid availability, environmental characteristics, regulatory constraints, and ease of implementation should also be considered. R1233zd(E) remains thermodynamically competitive because its net output is within 0.414 kW of that of R245fa; the other selection criteria require separate evaluation.

Figure 8 showed two design sensitivity curves for a trickle collector system coupled to a geothermal ORC, both recomputed on the common brine basis. Figure 8a showed that the solar contribution rose linearly with collector area and then flattened once the working fluid reached its own preheating temperature limit. Because every fluid received the same collector heat per unit area, the curves coincided before saturation and separated only at the plateau. Cyclopentane saturated first at 6.15% and 92.67 m^2, just above the 91.52 m^2 design field, whereas n-butane continued to 7.74% and 118.53 m^2. Figure 8b showed that the brine-only net power per unit brine flow increased with brine inlet temperature for every candidate, reaching 61.670 kW per kg/s for R245fa and 56.572 kW per kg/s for cyclopentane at the 188 °C design point. Solar heat is excluded from Figure 8b because the collector field delivers a fixed absolute duty that does not scale with the brine flow.

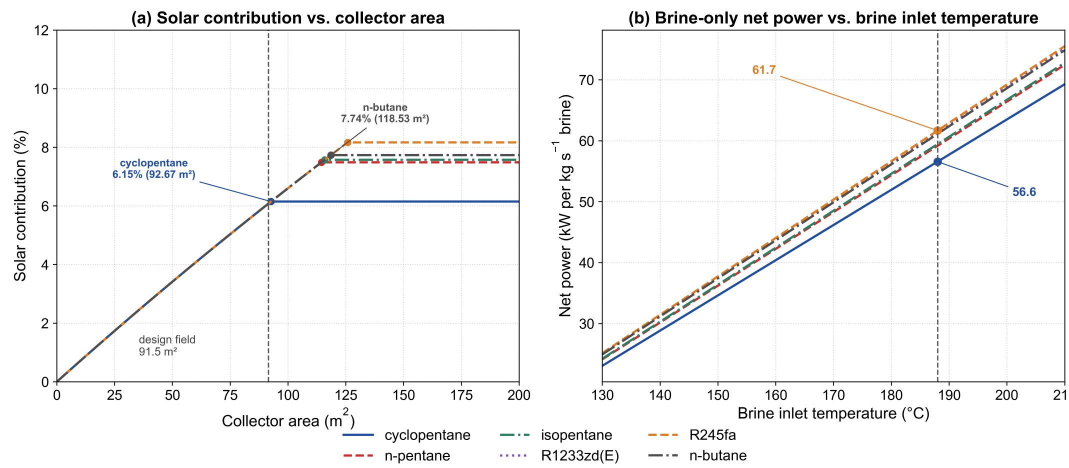

Figure 8. Design sensitivity of the trickle-collector system on the common brine basis: (a) solar contribution vs. collector area; (b) brine-only net power vs. brine inlet temperature

3.7 Transcritical CO_2 Comparison and Illustration of Supercritical Operation

Figure 9 compares the six subcritical organic working fluids with the two transcritical CO_2 cases on the common brine basis. As shown in Figure 9a, on the common brine basis, R245fa produced the highest net power at 110.961 kW, followed by R1233zd(E) at 110.547 kW, n-butane at 109.987 kW, isopentane at 106.955 kW, n-pentane at 106.473 kW, and cyclopentane at 101.788 kW. The same order was reproduced by the thermal efficiency in Figure 9b, which ranged from 14.983% for R245fa down to 13.744% for cyclopentane, and by the exergy efficiency in Figure 9c, where solar preheating raised every candidate by about two percentage points. Transcritical CO_2 was evaluated at two sink temperatures so that the comparison with the organic fluids was made on equal terms. At the 25 °C sink required for subcritical condensation, CO_2 produced 75.839 kW at a thermal efficiency of 10.903%, whereas at the same 30 °C sink used for the organic fluids it produced only 62.131 kW at 8.933%. Both cases required a very high operating pressure of 19.550 MPa to 21.763 MPa. The 25 °C result is therefore retained as a physically motivated sensitivity and not as evidence that CO_2 outperforms organic fluids, because the advantage disappears once the sink temperature is equalized.

R1233zd(E) was selected as a representative fluid for a qualitative comparison of subcritical and supercritical thermodynamic paths. Figures 10 and 11 use a 155 °C subcritical state and a 178 °C supercritical state to illustrate heating and expansion behavior; these representative diagram conditions are separate from the common-basis subcritical optimum used in Figures 7 and 9. In the T–s diagram, supercritical heating proceeds continuously without a discrete phase-change plateau, which can improve temperature matching between the brine and the working fluid.

Figure 10 shows the representative subcritical R1233zd(E) path at an evaporation temperature of 155 °C and the supercritical path at a turbine-inlet temperature of 178 °C. The trickle preheater raises the working fluid only during the initial heating stage, to a limit of 46.5 °C. Figure 11 shows the corresponding pressures: approximately 2.98 MPa for the subcritical high side, 3.73 MPa for the supercritical high side, and 0.155 MPa for the low side.

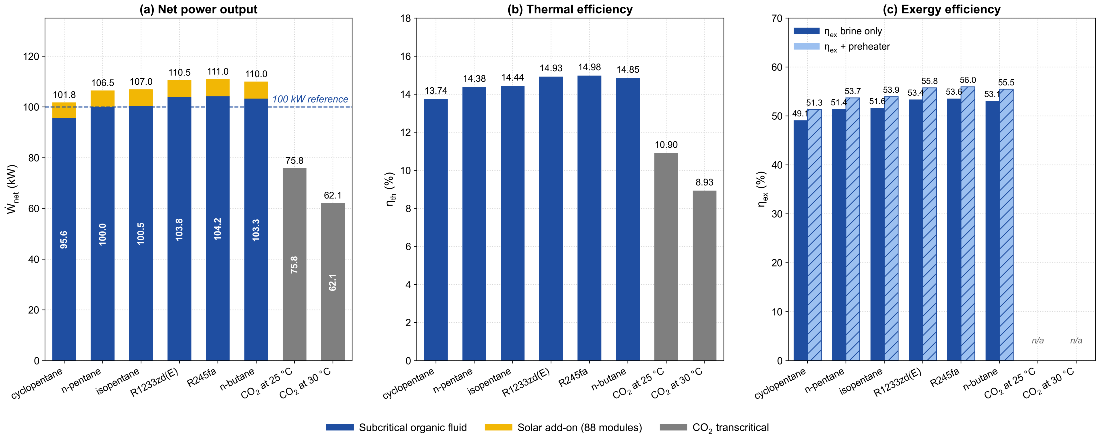

Figure 9. Working-fluid and transcritical CO_2 comparison on the common brine basis: (a) net power output; (b) thermal efficiency; (c) exergy efficiency

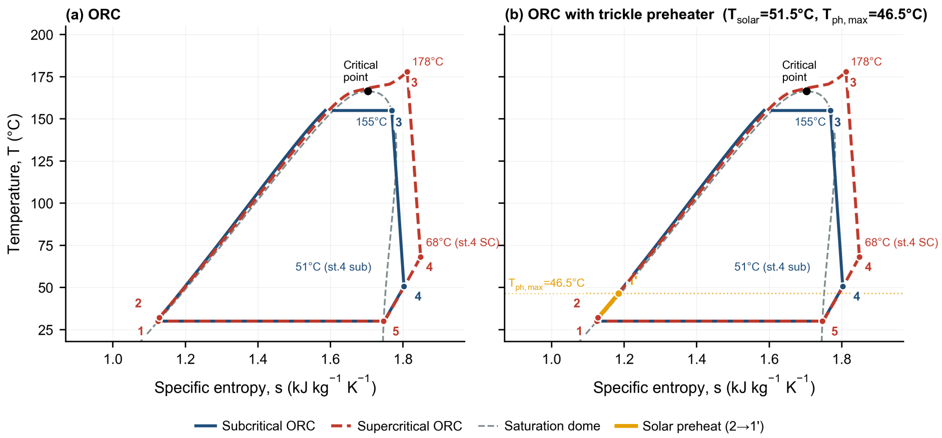

Figure 10. T-s diagram of R1233zd(E) under subcritical and supercritical modes

Note: ORC: organic Rankine cycle.

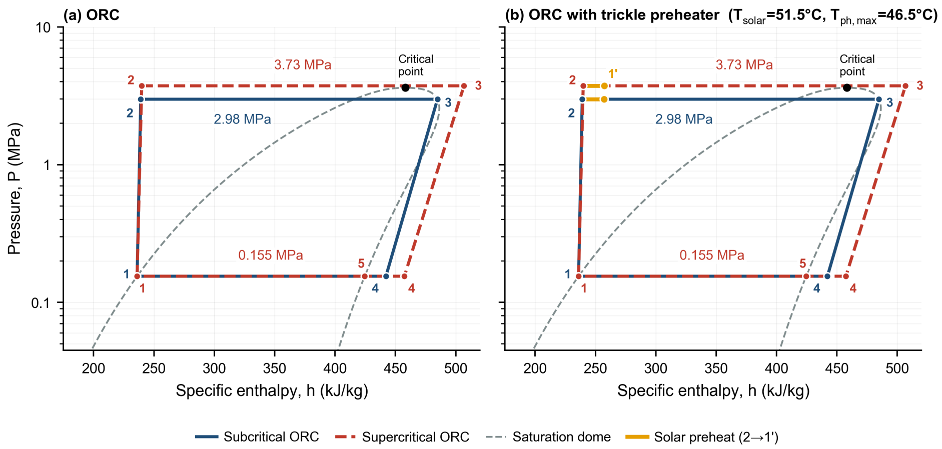

Figure 11. P-h diagram of R1233zd(E) under subcritical and supercritical modes

Note: ORC: organic Rankine cycle.

The illustrative diagrams show how supercritical heating changes the thermodynamic path when the fluid critical temperature is compatible with the available source temperature; they do not establish a common-basis performance advantage. In the quantified subcritical comparison at a geothermal-brine inlet temperature of 188 °C, R1233zd(E) ranked second. Transcritical CO_2 was less suitable under the evaluated conditions because of its high operating pressure, large back-work ratio, and strong sensitivity to sink temperature.

4 Conclusion

This study assessed the integration of a field-tested trickle solar collector as a preheater for a small-scale geothermal ORC. Experimental collector data were used directly as input to the thermodynamic model, and the solar-assisted cycle was evaluated under the same geothermal brine conditions as the reference cycle. Heat-transfer feasibility was verified over the complete counter-current temperature profile rather than solely at the terminal points.

The experimental collector reached a maximum outlet temperature of 51.5 °C, limiting the working-fluid temperature after the preheater to approximately 46.5 °C when a minimum heat-exchanger temperature difference of 5 °C was imposed. The collector was therefore more suitable for working-fluid preheating than for direct ORC evaporation. In the n-pentane reference case, 88 collector modules with a total aperture area of 91.52 m^2 supplied 45.024 kW of useful solar heat. This heat was fully transferred because it remained below the preheating temperature limit of 56.313 kW. Solar preheating increased the net power output from 100 to 106.473 kW, corresponding to an improvement of 6.473%, while the brine outlet remained at the prescribed reinjection temperature of 90 °C. The minimum approach temperature along the complete heating profile was 10.120 K, confirming the thermodynamic feasibility of the integrated configuration.

The thermal efficiency remained at 14.377% because solar preheating increased both heat input and power output without changing the principal cycle temperatures or component efficiencies. By contrast, the exergy efficiency increased from 51.393% to 53.705%, indicating more effective use of the combined geothermal and solar exergy inputs. Raising the assumed collector outlet temperature from 51.5 °C to 55–65 °C widened the allowable preheating range but did not increase the transferred heat or net power. Under the selected field configuration, system performance was limited by the useful heat supplied by the 88 modules rather than by the maximum preheating temperature. Further gains therefore require a larger collector area, greater useful heat output, or improved collector efficiency instead of a higher outlet temperature alone.

The comparison conducted under common brine and pinch constraints showed that R245fa produced the highest net power of 110.961 kW, followed closely by R1233zd(E) at 110.547 kW, whereas cyclopentane produced the lowest output among the six organic fluids at 101.788 kW. This result differed from the ranking obtained when each fluid was evaluated at an independent operating point, demonstrating the importance of applying a consistent geothermal source and complete temperature-profile constraint when screening ORC working fluids. Transcritical CO_2 was less suitable for the intermediate-temperature source because of its high operating pressure and large back-work ratio, producing only 62.131 kW at the same 30 °C heat-sink temperature used for the organic fluids.

These findings demonstrate that low-temperature trickle collectors can serve as technically feasible solar preheaters for increasing power recovery from geothermal brine without lowering the prescribed reinjection temperature. However, the present assessment combines collector-scale experimental measurements with system-level thermodynamic modeling rather than testing a fully integrated installation. Future work should therefore validate the coupled collector–preheater–ORC system under transient outdoor conditions, quantify experimental and operational uncertainties, improve the useful heat output of the collector field, and evaluate economic feasibility, pressure losses, fouling, control requirements, and long-term operating performance.

Author Contributions

Conceptualization, N.A.P.; methodology, N.A.P.; software, N.A.P.; formal analysis, I.M.G.; writing—original draft preparation, I.M.G.; writing—review and editing, S.; visualization, I.M.G.; supervision, S.; project administration, N.A.P.; funding acquisition, N.A.P. All authors have read and agreed to the published version of the manuscript.

Funding

This research was supported by the Directorate of Research and Community Service (DPPM) through the Fundamental Research (PF-DPPM) program (Grant No. 112/C3/DT.05.00/PL-MULTITAHUN LANJUTAN/2026 and 312.1/UN27.22/PT.01.03/2026).

Data Availability

The data used to support the research findings are available from the corresponding author upon request.

Acknowledgements

The authors thank the Institute for Research and Community Service (LPPM), Universitas Sebelas Maret, for administrative and institutional support.

Conflicts of Interest

The authors declare no conflicts of interest.

Declaration on the Use of Generative AI and AI-assisted Technologies

During the preparation of this work, the authors used AI (ChatGPT) to improve the language flow and refine grammatical structure. After using this tool/service, the authors reviewed and edited the content and take full responsibility for the content of the publication.

References

[1] X. Long, Q. Wang, B. Li, T. Gao, E. Xia, L. Sun, J. Wang, and H. Xie, "A critical review of technological advancements and challenges in geothermal power generation," *Renew. Sustain. Energy Rev.*, vol. 232, p. 116810, 2026. https://doi.org/10.1016/j.rser.2026.116810

[2] B. W. Kariuki, H. Hassan, M. Ahmed, and M. Emam, "A review on geothermal-solar hybrid systems for power production and multigeneration systems," *Appl. Therm. Eng.*, vol. 259, p. 124796, 2025. https://doi.org/10.1016/j.applthermaleng.2024.124796

[3] K. Li, C. Liu, S. Jiang, and Y. Chen, "Review on hybrid geothermal and solar power systems," *J. Clean. Prod.*, vol. 250, p. 119481, 2020. https://doi.org/10.1016/j.jclepro.2019.119481

[4] M. Astolfi, L. Xodo, M. C. Romano, and E. Macchi, "Technical and economical analysis of a solar-geothermal hybrid plant based on an organic Rankine cycle," *Geothermics*, vol. 40, no. 1, pp. 58–68, 2011. https://doi.org/10.1016/j.geothermics.2010.09.009

[5] N. Bist and A. Sircar, "Hybrid solar geothermal setup by optimal retrofitting," *Case Stud. Therm. Eng.*, vol. 28, p. 101529, 2021. https://doi.org/10.1016/j.csite.2021.101529

[6] B. Hu, J. Guo, Y. Yang, and Y. Shao, "Selection of working fluid for organic Rankine cycle used in low temperature geothermal power plant," *Energy Rep.*, vol. 8, pp. 179–186, 2022. https://doi.org/10.1016/j.egyr.2022.01.102

[7] S. Zhang, H. Wang, and T. Guo, "Performance comparison and parametric optimization of subcritical organic Rankine cycle (ORC) and transcritical power cycle system for low-temperature geothermal power generation," *Appl. Energy*, vol. 88, no. 8, pp. 2740–2754, 2011. https://doi.org/10.1016/j.apenergy.2011.02.034

[8] Q. Liu, F. Yang, X. Liu, X. Zhang, and Z. Yang, "Thermo-economic evaluation and working fluid screening for supercritical ORCs driven by medium-temperature geothermal sources," *Renew. Energy*, vol. 257, p. 124795, 2026. https://doi.org/10.1016/j.renene.2025.124795

[9] S. Hu, Z. Yang, J. Li, and Y. Duan, "Thermo-economic optimization of the hybrid geothermal-solar power system: A data-driven method based on lifetime off-design operation," *Energy Convers. Manag.*, vol. 229, p. 113738, 2021. https://doi.org/10.1016/j.enconman.2020.113738

[10] A. Bozkurt, M. S. Genç, and S. S. Seyitoğlu, "7E analysis of a low-temperature geothermal and solar energy integrated hybrid system for sustainable power and hydrogen generation," *Therm. Sci. Eng. Prog.*, vol. 66, p. 104073, 2025. https://doi.org/10.1016/j.tsep.2025.104073

[11] Z. Ge, X. Chen, J. Li, M. Yu, and F. Yang, "Thermodynamic and economic multi-objective optimization of geothermal and solar combined power system," *Results Eng.*, vol. 28, p. 108057, 2025. https://doi.org/10.1016/j.rineng.2025.108057

[12] D. Li, Z. Rao, Q. Zhuo, R. Chen, X. Dong, G. Liu, and S. Liao, "Resource endowments effects on thermal-economic efficiency of ORC-based hybrid solar-geothermal system," *Case Stud. Therm. Eng.*, vol. 52, p. 103739, 2023. https://doi.org/10.1016/j.csite.2023.103739

[13] S. Podlasek, M. Jankowski, P. Bałazy, K. Lalik, and R. Figaj, "Application of ANN control algorithm for optimizing performance of a hybrid ORC power plant," *Energy*, vol. 306, p. 132082, 2024. https://doi.org/10.1016/j.energy.2024.132082

[14] H. Ghasemi, E. Sheu, A. Tizzanini, M. Paci, and A. Mitsos, "Hybrid solar-geothermal power generation: Optimal retrofitting," *Appl. Energy*, vol. 131, pp. 158–170, 2014. https://doi.org/10.1016/j.apenergy.2014.06.010

[15] M. Ayub, A. Mitsos, and H. Ghasemi, "Thermo-economic analysis of a hybrid solar-binary geothermal powerplant," *Energy*, vol. 87, pp. 326–335, 2015. https://doi.org/10.1016/j.energy.2015.04.106

[16] A. Shaghaghi, F. Honarvar, M. Jafari, A. Solati, R. Zahedi, and M. Taghitahoone, "Thermodynamic and thermoeconomic evaluation of integrated hybrid solar and geothermal power generation cycle," *Energy Convers. Manag. X*, vol. 23, p. 100685, 2024. https://doi.org/10.1016/j.ecmx.2024.100685

[17] A. Atiz, H. Karakilcik, M. Erden, and M. Karakilcik, "Investigation energy, exergy and electricity production performance of an integrated system based on a low-temperature geothermal resource and solar energy," *Energy Convers. Manag.*, vol. 195, pp. 798–809, 2019. https://doi.org/10.1016/j.enconman.2019.05.056

[18] A. Erdogan, C. O. Colpan, and D. M. Cakici, "Thermal design and analysis of a shell and tube heat exchanger integrating a geothermal based organic Rankine cycle and parabolic trough solar collectors," *Renew. Energy*, vol. 109, pp. 372–391, 2017. https://doi.org/10.1016/j.renene.2017.03.037

[19] M. Alrbai, A. Al Masri, S. Abu-Dabaseh, M. Abusorra, and H. Hayajneh, "Thermodynamic assessment of hybrid solar-geothermal organic Rankine cycle: An exergy and energy-based analysis," *Energy Explor. Exploit.*, vol. 43, no. 4, pp. 1729–1759, 2025. https://doi.org/10.1177/01445987251329373

[20] M. Alibaba, R. Pourdarbani, M. H. Khoshgoftar Manesh, I. Herrera-Miranda, I. Gallardo-Bernal, and J. L. Hernández-Hernández, "Conventional and advanced exergy-based analysis of hybrid geothermal-solar power plant based on ORC cycle," *Appl. Sci.*, vol. 10, p. 5206, 2020. https://doi.org/10.3390/app10155206

[21] R. F. Rizal and M. Munir, "Enhancing the sustainability of PVT systems through optimized PCM selection and container configuration: A CFD approach," *Power Eng. Eng. Thermophys.*, vol. 3, no. 4, pp. 266–278, 2024. https://doi.org/10.56578/peet030404

[22] L. Q. Zhao, H. Li, N. Z. Jiang, T. L. Hong, Y. Mao, and Y. Y. Wang, "Advances in waste heat recovery technologies for SOFC/GT hybrid systems," *Power Eng. Eng. Thermophys.*, vol. 4, no. 1, pp. 12–29, 2025. https://doi.org/10.56578/peet040102

[23] N. A. Pambudi, I. R. Nanda, A. E. Putri, R. N. Salsala, M. Aziz, B. Rudiyanto, and A. Wiyono, "An experimental investigation of various trickle collector structures to enhance solar water heater efficiency," *Clean. Eng. Technol.*, vol. 21, p. 100789, 2024. https://doi.org/10.1016/j.clet.2024.100789

[24] N. A. Pambudi, I. R. Nanda, and A. D. Saputro, "The energy efficiency of a modified V-corrugated zinc collector on the performance of solar water heater (SWH)," *Results Eng.*, vol. 18, p. 101174, 2023. https://doi.org/10.1016/j.rineng.2023.101174

[25] D. Gonidaki and E. Bellos, "A detailed review of organic Rankine cycles driven by combined heat sources," *Energies*, vol. 18, no. 3, p. 526, 2025. https://doi.org/10.3390/en18030526

[26] G. Valencia Ochoa, E. V. Ortiz, and J. D. Forero, "Thermo-economic and environmental optimization using PSO of solar organic Rankine cycle with flat plate solar collector," *Heliyon*, vol. 9, no. 3, p. e13697, 2023. https://doi.org/10.1016/j.heliyon.2023.e13697

[27] I. H. Bell, J. Wronski, S. Quoilin, and V. Lemort, "Pure and pseudo-pure fluid thermophysical property evaluation and the open-source thermophysical property library CoolProp," *Ind. Eng. Chem. Res.*, vol. 53, no. 6, pp. 2498–2508, 2014. https://doi.org/10.1021/ie4033999

[28] A. Hribernik and T. Markovič Hribernik, "Techno-economic model for a quick preliminary feasibility evaluation of organic Rankine cycle applications," *J. Sustain. Dev. Energy Water Environ. Syst.*, vol. 9, no. 1, p. 1080336, 2021. https://doi.org/10.13044/j.sdewes.d8.0336

Nomenclature

A_c	Collector aperture area
$c_{p,w}$	Specific heat capacity of water
f_{derating}	Collector derating factor
G_T	Solar irradiance on the collector plane
h	Specific enthalpy
$h_{\mathrm{in}}, h_{\mathrm{out}}$	Inlet and outlet specific enthalpy
N_{modul}	Number of collector modules
P	Pressure
P_{crit}	Critical pressure of the working fluid
q_u''	Collector useful heat flux
s	Specific entropy
$s_{\mathrm{in}}, s_{\mathrm{out}}$	Inlet and outlet specific entropy
T_0	Ambient/dead-state temperature
$T_{\mathrm{brine,in}}$	Brine inlet temperature
$\varepsilon_{\mathrm{HX}}$	Heat-exchanger effectiveness

ρ_1	Working-fluid density at condenser outlet
PG	Net power gain
ψ_{dest}	Exergy destruction ratio
$\dot{E}x_{\mathrm{in,total}}$	Total exergy input rate
$T_{solar,\mathrm{out}}$	Solar collector outlet temperature
$T_{\mathrm{turb,in}}$	Turbine inlet temperature
$T_{\mathrm{WF,max}}$	Maximum working-fluid temperature after preheater
ΔT_{min}	Specified minimum heat-exchanger temperature difference
$\Delta T_{\mathrm{min,calc}}$	Minimum approach calculated along a heat-transfer profile
$\dot{E}x$	Exergy rate
$\dot{m}$	Mass flow rate
$\dot{Q}$	Heat transfer rate
$\dot{W}$	Power/work rate
η_{col}	Collector thermal efficiency
η_{ex}	Exergy efficiency
η_{pump}	Pump isentropic efficiency
η_{th}	Thermal efficiency
η_{turb}	Turbine isentropic efficiency
$T_{\mathrm{in}}, T_{\mathrm{out}}$	Collector inlet and outlet temperatures
SF	Solar fraction based on total heat input
SF_{brine}	Solar fraction relative to brine heat input
$w_{\mathrm{net,brine}}$	Specific net power per brine mass flow rate
$\Delta\dot{W}_{\mathrm{net}}$	Net power difference